PCCP



View Article Online **PAPER**



Cite this: Phys. Chem. Chem. Phys., 2022, 24, 13831

High throughput chirped pulse Fourier-transform microwave spectroscopy of ethanol and water clusters*

S. E. Dutton p and G. A. Blake*

Received 3rd March 2022. Accepted 13th May 2022

DOI: 10.1039/d2cp01055k

rsc.li/pccp

Here we discuss the design and performance of a novel high-throughput instrument for Chirped Pulse Fourier-transform Microwave (CP-FTMW) spectroscopy, and demonstrate its efficacy through the identification of the lowest energy conformers of the ethanol trimer and mixed water: ethanol trimers. Rotational constants for these trimers were calculated from observed lines in the spectra from 10 to 14 GHz, and compared to the results of anharmonic ab initio computations. As predicted, all trimers share a cyclic donor-acceptor hydrogen bonding structure, with the ethanol monomer favoring the gauche conformation in the lowest energy structures. The increased speed of data collection and resulting sensitivity opens a new avenue into rotational studies of higher order clusters.

1 Introduction

Small molecule clusters, though simple in their nature as modest-atom systems, are host to a number of open questions in physical chemistry. One need only examine the long-standing debate surrounding the nature of the hydrogen bond – a topic introduced in introductory chemistry courses - to see the mysteries still encapsulated in the dynamics of few molecule systems.

The hydrogen bond is of vast importance to physical, chemical and biological processes on earth, bottle-necking reaction rates in the atmosphere and determining solvation interactions in condensed phases.^{1,2} The importance of this motif is in part due to the weak nature of the hydrogen bond (4 to 40 kcal mol⁻¹), allowing bonds to break and form easily.¹

A specific area of interest addresses the behavior of hydrogen bonding interactions in alcohol-water mixtures. Condensed phase mixtures of alcohols such as ethanol and water display intriguing behavior, including their negative entropy of mixing. This is indicative of incomplete mixing on a microscopic scale.3-5 This behavior has not yet been fully characterized or understood, and the impacts of these properties are far reaching; for example, recent publications investigate the relevance of these physicochemical anomalies to hand-sanitizer effectiveness against COVID-19.6,7

Division of Chemistry and Chemical Engineering, California Institute of Technology, 1200 E California Blvd., Pasadena, CA 91125, USA. E-mail: gab@gps.caltech.edu † Electronic supplementary information (ESI) available. See DOI: https://doi.org/ 10.1039/d2cp01055k

To empirically elucidate the clustering behavior that gives rise to this microaggregation of water and alcohol, the structure determination of small clusters of alcohol and water is a useful proxy system to elucidate the dynamics of bulk mixtures. In the present work, small clusters of ethanol and water are studied, so that accurate structural information may be used to build up to fully molecular bulk models of ethanol and water mixing.

One consideration specific to ethanol clusters, that adds further complexity to accurate modeling, is trans versus gauche conformational variation. Previous studies have demonstrated that weak hydrogen bonding in ethanol and water clusters may additionally stabilize the gauche conformation over the trans,8 which is favored for the monomer. Computational studies of the ethanol trimer have shown a similar trend, with a number of low energy structures with both the trans and gauche conformation of one or more monomers. 9,10

To characterize the potential energy surfaces pertaining to such clusters, Chirped Pulse Fourier-Transform MicroWave (CP-FTMW) spectroscopy has become the main tool for the high resolution rotational spectroscopy of gaseous species. Invented by the Pate group at the University of Virginia, 11 many previous studies have demonstrated the efficacy of this technique for high-sensitivity measurements of pure rotational spectra from cm to (sub)mm wavelengths.^{8,12–15}

One challenge in past studies with this approach is that sensitivity can be limited by both the pumping speed and by the capabilities of chirp and signal acquisition digital electronics, requiring that gas be pulsed into the chamber to avoid collisional broadening or destruction of clusters from high pressures in the vacuum chamber.^{8,16–18} Pulsed gas expansions are effective, but most have a duty cycle of only a few percent.

In this work, a continuous, large aperture expansion instrument for CP-FTMW is presented, and compared to pulsed instruments. The efficacy of this technique is further demonstrated through the study of the ethanol trimer and mixed water: ethanol trimers. Rotational spectra and anharmonic ab initio calculations are used to guide the rotational constant assignments of the lowest energy conformers of the these clusters. We first turn to a description of the new instrument and results, before describing the nature of hydrogen bonding in the trimers.

2 Experimental methods

The high vacuum chamber design is specifically designed to permit a collinear orientation of the microwave horn and supersonic beam expansion. This orientation allows the same microwave horn to be used for both the broadcast and detection of MW radiation, and optimizes the interaction volume. This instrument is thus an alternative to the 'original' singlenozzle system, as opposed to a multi-nozzle system as implemented elsewhere.19

The high pumping speeds necessary for the desired experiments were achieved via a magnetically levitated Osaka TGKine 3304 Turbomolecular pump in series with an Edwards EM 275 Rotary Vacuum pump, which comes with an additional roughing pump. With this system, the base pressure in the chamber is roughly 10⁻⁹ torr, and the pumping speed for molecular nitrogen is $\sim 3400 \text{ L s}^{-1}$. For Ar or N₂ expansions, the maximum compression ratio is nearly 108 (for molecular hydrogen or He the compression ratio drops to 10³⁻⁴). With this high pumping speed, gas may be continually introduced into the chamber at 2 atm nozzle pressure without the background pressure rising above 4×10^{-4} torr, and the high compression ratios achievable mean quite modest backing pumps and roughing lines are required. The resulting mach disk distance, for a pinhole expansion, is at least 1 meter away from the nozzle, ensuring free expansion of the clusters without collisions, and imparting a new ability to probe cluster formation in continuous expansion conditions.

As described previously, we employ direct digital synthesis (DDS) (specifically the Analog Devices AD9914 board) to generate a 2 GHz chirp over 1.2 microseconds. 12 The pulse is lowpass filtered (Mini-Circuits VLP-24) and heterodyned with the local oscillator (LO) frequency from the output of Hewlett-Packard function generator (HP 83260B Series Swept Signal Generator) with a microwave circuit mixer (Marki MIR0726). The resulting pulse contains the sum and the difference of the LO frequency and the digitally generated broadband chirp.

The heterodyned pulse is amplified with a 40 watt solid state amplifier, or SSA (Microsemi RF Integrated Solutions Model LO618-46-T680), and passed through a circulator (Teledyne C-12S63T) to the microwave horn. A diagrammatic representation of the microwave circuit is depicted in Fig. 1. Note that this diagram does not accurately depict the geometry of the nozzle and gas expansion in the chamber.

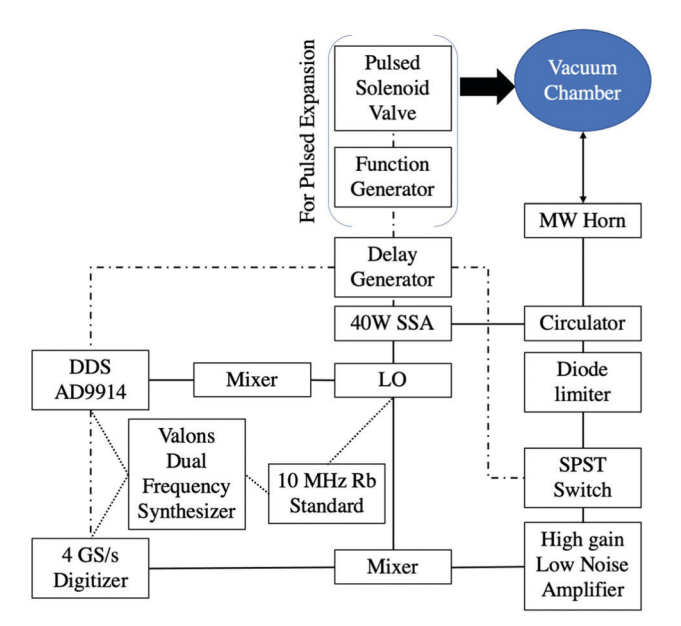


Fig. 1 Schematic of the microwave circuit built. Solid lines represent SMA cables transmitting the microwave signal. Dotted lines represent clocking signals, and dashed lines represent trigger signals

The entire circuit is triggered by a digital delay generator (Stanford Research Systems Model DG535 4 Channel Digital Delay Generator). For signal detection, a waveform is sent to an arbitrary waveform generator (Stanford Research Systems Model DS 340 15 MHz Frequency Generator) to trigger the AD9914 DDS board every 20 microseconds, so that an 18 microsecond FID is collected for each microwave pulse. The delay generator also triggers the solid state amplifier to amplify the signal for only the duration of the input pulse.

The detection electronics include a high-gain, low-noise amplifier (Miteq AMF-5F-08001800-14-10P), a mixer to downconvert the double-sideband signals (Marki MIR0726), and an Agilent digital-toanalog converter (DAC) board. This DAC board is clocked to the same external source as the DDS board, and samples the molecular FID at 4 GS s⁻¹. FID collection is triggered by the DDS board, and up to 10 million FIDs are averaged at a time before being written directly to text files. Critically, both the DDS board and the DAC board have low latency. This ensures high duty cycles even under continuous excitation and FID acquisition environments.

The system is clocked by a rubidium frequency standard (Stanford Research Systems Model FS725 Rubidium Frequency Standard), providing a time base for a Valon dual frequency synthesizer (Valon Technology LLC 5008) that is used as a reference for the DDS board and the digitizer. The rubidium standard also clocks the LO signal generator to ensure phase stability.

We have tested both pinhole and slit expansions. There is some concern about collisional broadening for the latter, as the pressure at the outlet of the slit decreases more slowly than in pinhole expansions, and because such collisions are clearly manifest in pulsed large aperture Laval nozzle expansions²⁰ used to study low temperature chemical kinetics. To confirm that the mach disk for the slit nozzle is sufficiently far from the

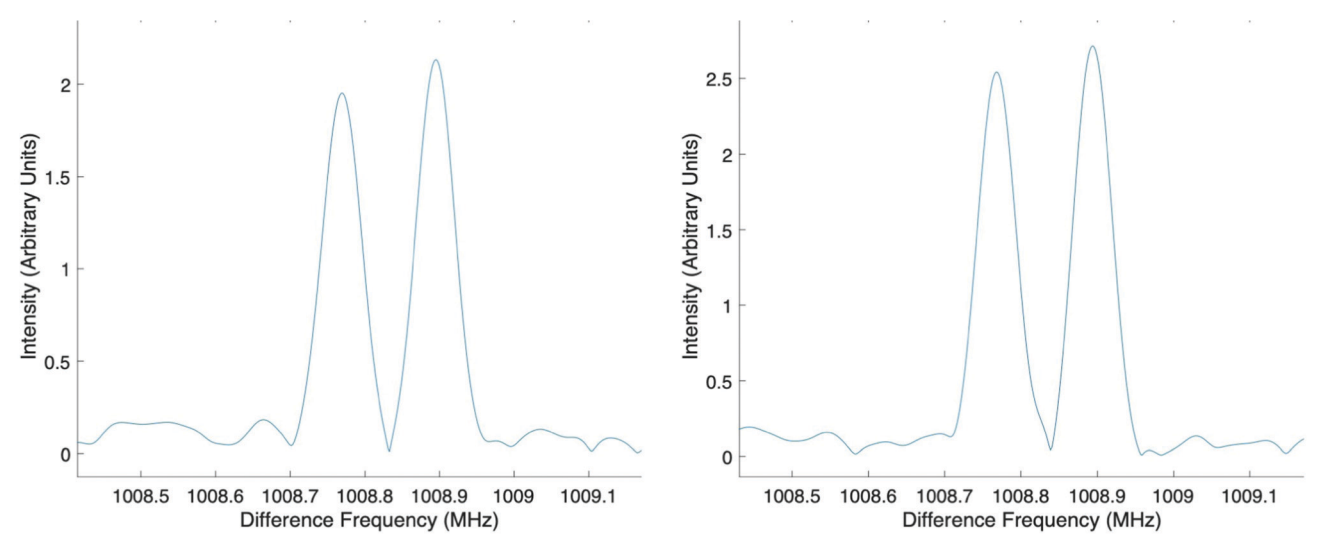


Fig. 2 Long FID (50 microsecond) collection for 1 mm diameter circular source (left) and a 10 cm × 25 μm slit nozzle (right) continuous expansions of Ethanol at 0.4 atm, 50 sccm flow. Longer FIDs result in resolution of the Doppler splitting of the ethanol dimer line at 1008 MHz offset from the 12.0 GHz LO frequency. Full width half max of each line is 60 KHz

slit, experiments with longer FID acquisitions were run. Normally, an FID of 18 microseconds is taken, as this maximizes the signal-to-noise ratio of the observed peaks in a given wall clock time. Longer FIDs optimize the spectral resolution, at the cost of reduced sensitivity.

To characterize the expansions, experiments with molecular FIDs of 50 microseconds were acquired for both the slit and point source nozzle. With Ar as the carrier gas (used for its rotational cooling²¹ and cluster generation efficiency) at 0.4 atm background pressure, a mixture of argon and ethanol was flowed continuously into the chamber at 50 sccm. Under these conditions, the pressure in the chamber hovered near 2.0×10^{-4} torr. With a 12.0 GHz LO field and 50 million averages collected, the full width half max (FWHM) of the strongest peaks was ~ 60 kHz for both the point source and the slit expansion, as shown in Fig. 2. These longer FIDs also reveal the expected Doppler splitting of transitions, a result of the emitted radiation propagating both towards the horn and away from it, then reflecting back in to the detection circuit.

The consistent width of the peaks for both the point source and slit nozzle expansions indicates that collisional broadening is not significant for either nozzle under these expansion conditions. At carrier gas background pressures exceeding 1 atm, initial experiments do show that the peaks from the slit nozzle are slightly wider than those from the point source nozzle, implying that this is the maximum background pressure for a slit nozzle continuous expansion to avoid collisional broadening of the pure rotational transitions of molecules and clusters in the molecular beam.

Results and discussion

3.1 Computational results

To aid in spectral assignments, ab initio calculations for the equilibrium and ground state rotational constants were carried

out with second order Møller-Plesset (MP2) perturbation theory using the 6-311++G(d,p) basis set with anharmonic corrections via the Gaussian 09 package. 22 This level of theory and basis set choice have previously been used in studies of the ethanol/ water dimer, and produce reasonably accurate rotational constants without taking prohibitively long to converge on modest clusters.8 Initial structures were generated based on chemical intuition and from comparison to studies in the literature.^{8,9} Images of the lowest energy structures for (C2H5OH)2H2O are shown in Fig. 3. The rotational constants from the converged structures were used to simulate spectra with the program PGOPHER.²³ These rotational constants are shown in the first column of Table 1 for the two lowest energy conformers of the ethanol trimer, and in Table 2 for the lowest energy conformers of the trimer formed between two ethanol molecules and one water molecule. Observed rotational lines were then fitted with the program SPFIT, 24 and the fitted rotational constants were compared to the ab initio results.

As expected from water cluster studies, the main motif of the trimers involves a cyclic pattern where all monomers accept and donate hydrogen bonds. The more subtle structures of interest here are conformers related to the orientation of the carbon groups with respect to the plane of hydrogen bonding. All spectra are rigid-rotor like, and it is not the goal of this work to capture modes associated with internal rotation. In addition, the height of barriers between conformers is not empirically

The ab initio energy difference between the two lowest energy conformers of both the pure ethanol and the mixed trimers is < 1 kcal mol⁻¹, and suggested that both conformers should be observable in experimental spectra. The ethanol subunits of both pure ethanol trimers and mixed trimers are all in the trans configuration in the isolated structures. However, as seen in Fig. 3, the orientation of the ethanol molecules relative to the plane of hydrogen bonding interactions varies

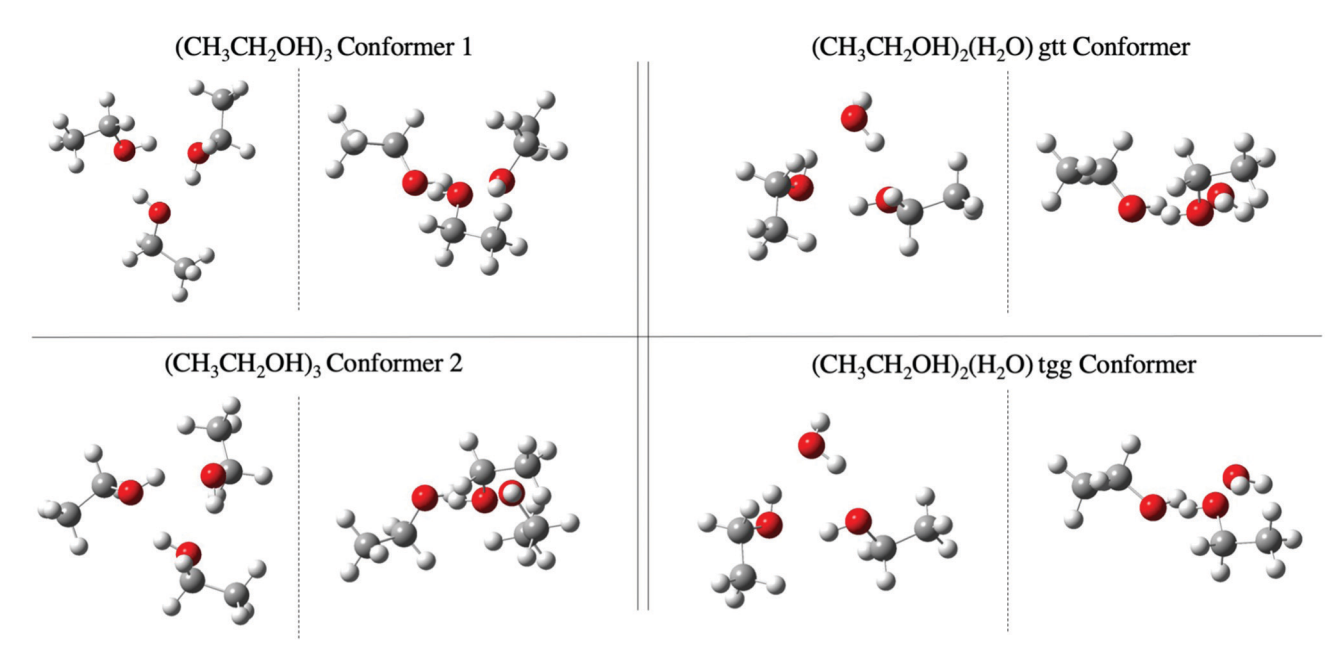


Fig. 3 The two lowest conformations for the pure ethanol trimers and those with two ethanol and one water monomer. The top row is the lowest energy conformation, that for the bottom row lies <1 kcal mol $^{-1}$ higher in energy. Optimized structures and rotational constants were determined viaGaussian 16 at the MP2 level of theory and 6311+G(d,p) basis set. The left column shows a 'top-down' view of the hydrogen bonding in the conformers, and the right column shows a 'side' view with respect to the hydrogen bonded cyclic motif, emphasizing the difference configuration of the ethanol carbon chains.

Table 1 Computational and experimentally determined rotational constants for the lowest energy conformer of the ethanol trimer. Parameters are fitted via SPFIT, using Watson's reduction of the Hamiltonian. N is the number of lines from the experimental spectrum fit, and the values in parentheses are the 1σ errors reported by SPFIT

	Ab initio conformer 1	Fitted conformer 1	Ab initio conformer 2	Fitted conformer 2
A/MHz	995.9	996.29 (4)	1015.8	1012.48 (4)
B/MHz	801.9	802.64 (10)	798.5	800.36 (22)
C/MHz	469.4	469.31 (21)	473.9	474.28 (18)
$D_{\rm I}/{ m kHz}$	2.33	15.12 (9)	2.11	-1.31(17)
$D_{\rm IK}/{ m kHz}$	-3.61	-47.6(3)	-3.25	-35.53(6)
$D_{\rm K}/{\rm kHz}$	1.49	36.42 (24)	1.34	41.17 (6)
d_1/kHz	-1.01	4.54 (4)	-0.841	13.78 (16)
d_2/kHz	-0.272	37.77 (24)	-0.170	77.10 (10)
μ_a/D	1.18	. ,	1.22	. ,
$\mu_{\rm b}/{ m D}$	-0.30		-0.28	
$\mu_{\rm c}/{\rm D}$	-0.14		0.17	
N		12		13
rms/kHz		56		96

Table 2 Calculated and experimentally determined rotational constants for the mixed water and ethanol trimers observed. Parameters are fitted via SPFIT, using Watson's reduction of the Hamiltonian. N is the number of lines from the experimental spectrum fit, and the values in parentheses are the 1σ errors reported by SPFIT

	Ab initio tgg	Fitted tgg	Ab initio gtt	Fitted gtt
A/MHz	2711.4	2709.38 (7)	2414.6	2406.62 (3)
B/MHz	922.7	923.47(17)	1069.7	1068.14 (7)
C/MHz	724.6	724.86 (13)	809.9	810.01 (16)
$D_{\rm I}/{ m kHz}$	0.719	20.9 (9)	2.55	151.7 (6)
$D_{\rm IK}/{ m kHz}$	-0.311	-54.2(26)	-5.66	-289.1(13)
$D_{\rm K}/{\rm kHz}$	17.9	31.1 (17)	13.6	135.9 (6)
d_1/kHz	-0.18733	-14.1(5)	-0.67	-58.70(26)
d_2/kHz	-0.03355	22.4 (12)	-0.07413	29.81 (21)
μ_a/D	0.69	()	1.17	()
$\mu_{\rm b}/{ m D}$	-0.48		-0.41	
$\mu_{\rm c}/{\rm D}$	0.073		0.14	
N		10		9
rms/kHz		117		82

between the conformations - the mixed ethanol and water trimers are shown as an example. In the top row, this conformer has a gauche relationship between the ethanol groups, and both ethanol molecules are trans to the water molecule. In contrast, the bottom row shows a conformer that is trans between the ethanol groups, and gauche relative to the water. The first mixed trimer configuration shown is referred to in this paper as "gtt", and the second is referred to as "tgg".

The two lowest energy structures calculated for the pure ethanol trimer both have two trans relationships between the ethyl groups, and one gauche. The lowest energy structure is labeled as Conformer 1, and the second lowest is labeled as Conformer 2. The energy difference between these structures is less than 1 kcal mol⁻¹. The lack of gauche conformation ethanol in all identified trimers implies that the stability afforded by additional hydrogen bonding interactions is less than the energy cost of overlapping ethanol groups. Further study of neat and mixed water: ethanol trimer isotopologues would help elucidate this trend (Fig. 3).

3.2 Experimental results

PCCP

Experimental spectra were recorded for pure ethanol and for a mixed expansion of ethanol and water. Experiments with 0.7 atm background pressure of argon, 50 secm gas flow, and an 18 microsecond FID collection time achieved a signal-tonoise (S/N) ratio of 830:1 for lines assigned to the ethanol trimer, with a full width half max (FWHM) of 100 kHz. For the mixed trimers, the S/N ratio was ~80:1 for the strongest identified lines, with the same FWHM as the ethanol trimer lines. Spectra collected under these conditions with LO settings of 11.6 to 12.1 GHz and from 17.5 to 17.6 GHz were compared with the spectrum generated from the ab initio calculated rotational constants using PGOPHER for line assignment. Data sets were processed by removing known lines of the ethanol monomer, water monomer, and pure and mixed dimers of each from the spectrum. The spectroscopic accuracy and precision, and FWHM trends, were bench marked by comparison to known lines of the ethanol monomer, values for which were obtained from the JPL Molecular Spectroscopy Database, 25 and are commensurate with previous experimentation in the Blake lab, as described in the methods. See Fig. 4 for example spectra.

Lines observed in the spectrum were then fitted with SPFIT to generate calculated rotational constants, shown in Table 1 for the ethanol trimer and Table 2 for the mixed trimers. The

trimers of interest are locked in a circular H-bond motif, meaning that the current work focuses on distinguishing between various conformations of this locked H-bond motif, as opposed to different bonding structures.

By comparison to these spectra simulated with PGOPHER, the rotational temperature of the clusters was estimated to be 10 K. At this temperature, there were between 15 to 30 strong rotational lines in the spectral range of the experiment for each type of cluster. At least half of the strong lines expected to be observed were fit to calculate the rotational constants from experimental spectra. Specifically, 12/25 lines were fit for conformer 1, and 13/20 lines were fit for conformer 2 of the pure ethanol trimers. For the mixed trimers, 10/20 lines were fit for tgg, and 9/20 lines were fit for gtt.

Of these lines fit for each trimer, most were a-type rotational transitions, as expected from the relative magnitude of the A, B, and C rotational constants and the electric dipole projections. First, these a-type transitions were fit. Next, at least one b-type and c-type transition were fit for each trimer to help improve the fit of the experimental constants. To more accurately assign these weaker c-type transitions, the chirp bandwidth was reduced to 1 GHz, enhancing the molecular polarization, and thus FID intensity, with the available amplifier output. This increased power density was essential in assigning the lower

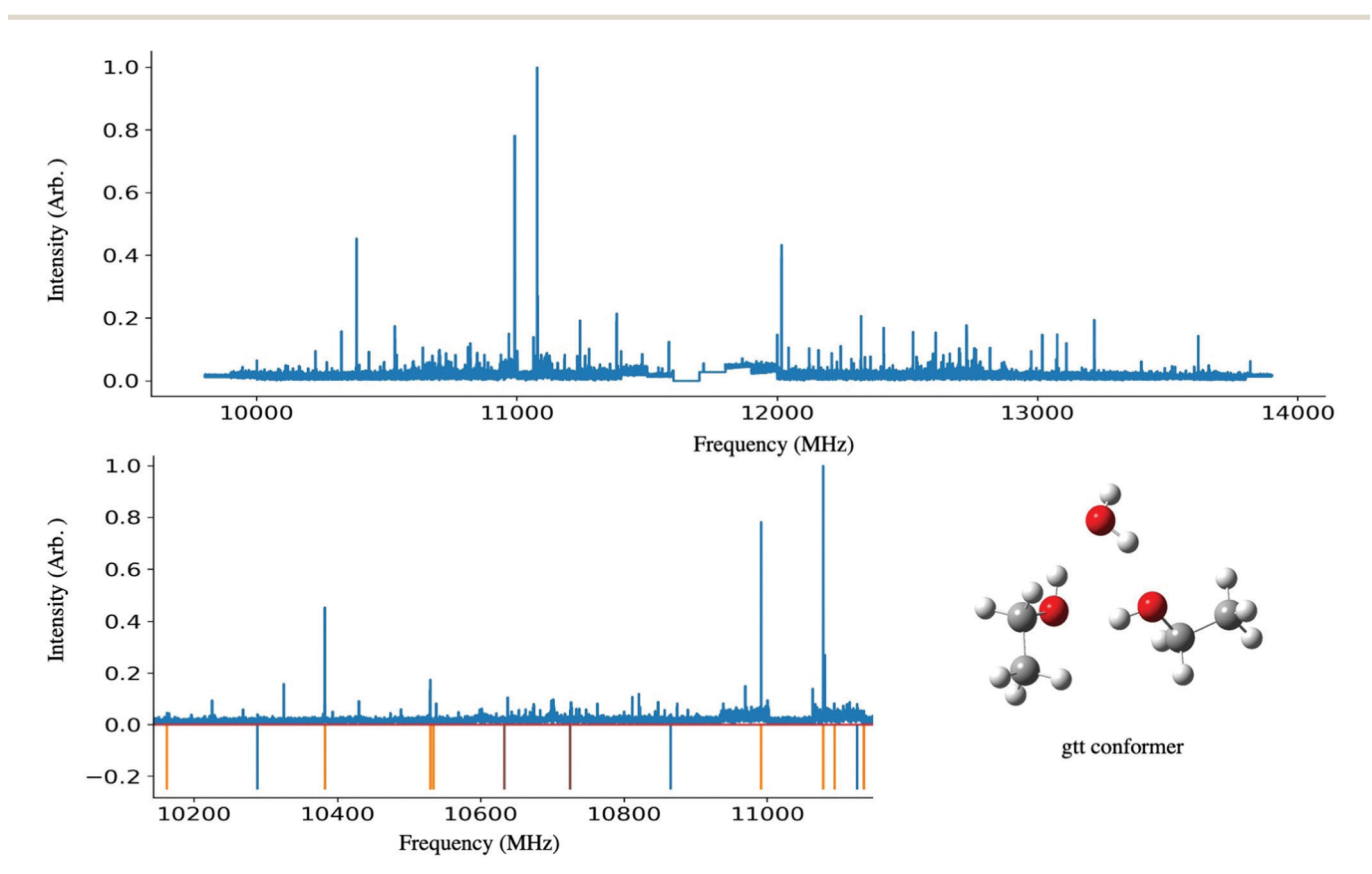


Fig. 4 Example of the experimental spectra collected on the mixed expansion of water and ethanol. On top is the full bandwidth collected, the bottom spectrum shows an inset of this spectrum with lines fitted for pure ethanol monomer (orange), water monomer (red), ethanol/water dimer (green), ethanol trimer (brown), and the mixed trimer of the up/down configuration (blue). The full spectrum is 200 million averages each of 6 LO settings, corresponding to approximately 13 hours of data collection. To right is the gtt conformer for reference.

Paper

intensity c-type transitions, for which only the strongest predicted transitions were sought for, and fit, with relative intensity of 70% of the a-type spectral lines. All key transition assignments were verified with dual resonance experiments.

Rigid rotor fit r.m.s. values were higher than previous work, at ~ 100 kHz, which is mostly likely explained by internal rotations of the methyl subgroups splitting the observed rotational transitions. The barrier to rotation for these methyl subgroups was calculated to be ~1100 cm⁻¹ using ab initio techniques with Gaussian. As seen in previous work, coupling to large amplitude motion of the trimer will effectively lower the barrier to internal rotation of the methyl groups, which would result in increased internal rotation splittings, and result in increased r.m.s. to the overall fits since in this case the pure all A-state combinations of the tops cannot be separated from mixed A-E and E-E states. 26-28

To assess the likely size and nature of the line splittings associated with the modest barriers to internal rotation, the trimer spectra were modeled with the internal rotation fitting program XIAM.29 The results indicate that for rotational mode splittings of up to 100 kHz, approximately the largest residuals in the rigid rotor fits, to lines most susceptible to internal rotation perturbations, a barrier to internal rotation of approximately 1000 cm⁻¹ is needed. Thus, the magnitude of the barrier is only modestly lowered by coupling to the other large amplitude motions of the cluster, as expected due to the interlocked donor-acceptor nature of the trimers. In addition, the sign of the error between the SPFIT model and XIAM agrees, supporting the plausibility of the internal rotation fitting.

This magnitude of splitting is too small to be resolved, even with longer FID collection (~ 50 microseconds), with the present instrument, although the asymmetry in both peak shape and relative intensity of Doppler splitting observed in the line shapes of these long FID experiments supports this magnitude of splitting due to internal rotation. Quantitative studies of these splittings would require a large cavity, coaxial geometry Flygare machine, and is beyond the scope of the present work. Simple order-of-magnitude estimates of the offsets of the A symmetry transitions from the peaks of the internal rotation envelopes with the current instrument lower the fit r.m.s. by factors of 2-3, as discussed in the ESI†.

Importantly, this increased error does not influence the line assignment; the various conformers observed have larger spectral differences than the r.m.s. error of the fits, and the lines included in these fits have been verified with dual resonance experiments. Thus, we are confident in the assignment of lines to different conformers and the geometric differences of these conformers that give rise to the spectral variation observed. This demonstrates the improvement in sensitivity of the current instrument over previous work, and opens the door for further projects investigating conformational variation in high order clusters.

As discussed in the experimental section, the most impactful change in this system was the integration of a high speed, high compression ratio turbomolecular pump into the experimental chamber, coupled to high speed/high duty cycle digital electronics. Compared to previous CP-FTMW experimentation, this single change increased the duty cycle of the system from $\sim 1\%$ to upwards of 70%, thanks to the new capability to introduce gas continuously into the chamber without overloading the pumps, and with no pressure broadening of the rotational spectra due to the low background pressure enabled by the uniquely high compression ratios achieved with high throughput turbomolecular pumps. The higher duty cycle resulting from continuous expansion thus led to decreased lab time required for experimentation, altogether speeding up the data collection process. The signal to noise ratio of 830:1 achieved here for the ethanol trimers was the result of 13 hours of averaging; the former incarnation of this instrument achieved a signal to noise ratio of ~200:1 on the peaks of interest after 40 hours of averaging. 12,30 Thus, though a modest technological innovation, the increased pumping speed has dramatic impact on the speed and ease of experimentation. In addition, the implementation of continuous throughput high duty cycle experiments combined with a slit expansion geometry have allowed for novel clusters to be identified. Importantly, the slower fall off in beam density enables improved cluster generation efficiencies, especially for higher order clusters. For example, with an SNR of more than 100:1 for water hexamer lines, compared to a previous SNR of 15:1 in the same wall clock time, the high pumping speed and low background enabled by the turbomolecular pump provides an optimal environment for the rotational study of clusters, where large interaction volumes are pivotal.

This arises because under similar expansion and excitation conditions, the sensitivity of a chirp pulse instrument depends on the noise figure of the detection circuit and the number of FIDs averaged. For a given instrumental noise figure and chirp bandwidth, because the turbopump enables continuous expansions to be run, at least for dimers and trimers, under conditions that match cluster generation efficiency in pulsed operation, no sensitivity is lost with high duty cycle DAC systems. That is, there is no difference in the number of microwave pulses needed to achieve a given S/N, but the time required to achieve it is decreased by the increased sample consumption per unit wall clock time. With commercially available high power amplifiers and multi-card DAC systems analog bandwidths of > 10 GHz can be acquired and averaged on the fly. Thus, on balance, it is the view of the authors that the increased rate of material consumption per unit time does not necessarily imply high sample consumption rates, and with sufficiently high bandwidth DAC systems is entirely consistent with isotopically enriched sample studies for structural determination. This conclusion may not be valid for large clusters of low volatility species, which will likely require stringent, very high pressure expansion conditions, but should true for a very wide range of substances of chemical interest. And, the improved clustering efficiency of the slit expansion leads to good sensitivity to larger clusters. For example, with the current system, methanol and methanol-water clusters up to the hexamers are readily seen, as will be described in future publications.

4 Conclusions

The observed ethanol trimer and mixed ethanol and water rotational spectra demonstrate the effectiveness of ab initio calculations for predicting structures and rotational constants of this class of small molecule clusters. The computed and fitted rotational constants are relatively close in value, reflecting the accuracy of the ab initio methods. This accuracy is consistent with the rigid structure of the hydrogen bonding ring in these trimers; the stability afforded by the uniform hydrogen bond donor and acceptor configuration 'locks' the geometry into conformation, making the potential energy surface of these trimers steeper between conformers and allowing calculational methods to more easily, and accurately, predict structural parameters.

This work has also served to demonstrate the efficacy of this new instrument for rotational studies of small molecule clusters. The high throughput afforded by the increased pumping speed of the turbomolecular pump decreases the lab time required for experimentation by a factor of ten over previous instruments, and the high compression ratio enables modest backing pumps and roughing lines to be used. This efficiency expands the scope of potential research targets, as demonstrated herein with the identification of mixed water: ethanol trimers in a dense rotational spectrum. Future work in this area will benefit from the speed of data collection with continuous expansion, and will work to identify similarly difficult to isolate small molecule clusters.

Conflicts of interest

There are no conflicts to declare.

Acknowledgements

The authors gratefully acknowledge support from the NSF CSDM-A program (Grant CHE-1665467) and the NASA Laboratory Astrophysics program (Grant NNX-16AC75G). SED is supported by the National Science Foundation Graduate Research Fellowship Program under Grant no. DGE-1745301. Any opinions, findings, and conclusions or recommendations expressed in this material are those of the authors and do not necessarily reflect the views of the National Science Foundation.

Notes and references

- 1 G. R. Desiraju, The weak hydrogen bond: in structural chemistry and biology, Oxford University Press, Oxford New York, 1999.
- 2 J. H. Seinfeld and S. N. Pandis, Atmospheric chemistry and physics: from air pollution to climate change, John Wiley & Sons, 3rd edn, 2016.
- 3 I. Juurinen, K. Nakahara, N. Ando, T. Nishiumi, H. Seta, N. Yoshida, T. Morinaga, M. Itou, T. Ninomiya, Y. Sakurai,

- E. Salonen, K. Nordlund, K. Hämäläinen and M. Hakala, Phys. Rev. Lett., 2011, 107, 197401.
- 4 A. K. Soper, L. Dougan, J. Crain and J. L. Finney, J. Phys. Chem. B, 2005, 110, 3472-3476.
- 5 S. Lenton, N. H. Rhys, J. J. Towey, A. K. Soper and L. Dougan, J. Phys. Chem. B, 2018, 122, 7884-7894.
- 6 N. N. Nyamweya and K. O. Abuga, 2021.
- 7 K. Abuga and N. Nyamweya, Pharmacy, 2021, 9, 64.
- 8 I. A. Finneran, P. B. Carroll, M. A. Allodi and G. A. Blake, Phys. Chem. Chem. Phys., 2015, 17, 24210-24214.
- 9 A. Malloum, J. J. Fifen and J. Conradie, Phys. Chem. Chem. Phys., 2020, 22, 13201-13213.
- 10 M. Masella and J. P. Flament, J. Chem. Phys., 1998, 108, 7141-7151.
- 11 G. G. Brown, B. C. Dian, K. O. Douglass, S. M. Gever, S. T. Shipman and B. H. Pate, Rev. Sci. Instrum., 2008, 79, 053103.
- 12 I. A. Finneran, D. B. Holland, P. B. Carroll and G. A. Blake, Rev. Sci. Instrum., 2013, 84, 083104.
- 13 G. J. Mead, E. R. Alonso, I. A. Finneran, P. B. Carroll and G. A. Blake, J. Mol. Spectrosc., 2017, 335, 68-73.
- 14 B. C. Dian, G. G. Brown, K. O. Douglass and B. H. Pate, Science, 2008, 320, 924-928.
- 15 L. Evangelisti, G. Sedo and J. van Wijngaarden, J. Phys. Chem. A, 2011, 115, 685-690.
- 16 C. Puzzarini, J. F. Stanton and J. Gauss, Int. Rev. Phys. Chem., 2010, 29, 273-367.
- 17 C. Calabrese, B. Temelso, I. Usabiaga, N. A. Seifert, F. J. Basterretxea, G. Prampolini, G. C. Shields, B. H. Pate, L. Evangelisti and E. J. Cocinero, Angew. Chem., Int. Ed., 2021, 16894-16899.
- 18 E. M. Neeman and T. R. Huet, Phys. Chem. Chem. Phys., 2021, 23, 2179-2185.
- 19 J. L. Neill, K. O. Douglass, B. H. Pate and D. W. Pratt, Phys. Chem. Chem. Phys., 2011, 13, 7253.
- 20 J. M. Oldham, C. Abeysekera, B. Joalland, L. N. Zack, K. Prozument, I. R. Sims, G. B. Park, R. W. Field and A. G. Suits, J. Chem. Phys., 2014, 141, 154202.
- 21 E. J. Campbell, L. W. Buxton, T. J. Balle, M. R. Keenan and W. H. Flygare, J. Chem. Phys., 1981, 74, 829-840.
- 22 M. J. Frisch, G. W. Trucks, H. B. Schlegel, G. E. Scuseria, M. A. Robb, J. R. Cheeseman, G. Scalmani, V. Barone, B. Mennucci, G. A. Petersson, H. Nakatsuji, M. Caricato, X. Li, H. P. Hratchian, A. F. Izmaylov, J. Bloino, G. Zheng, J. L. Sonnenberg, M. Hada, M. Ehara, K. Toyota, R. Fukuda, J. Hasegawa, M. Ishida, T. Nakajima, Y. Honda, O. Kitao, H. Nakai, T. Vreven, J. A. Montgomery, Jr., J. E. Peralta, F. Ogliaro, M. Bearpark, J. J. Heyd, E. Brothers, K. N. Kudin, V. N. Staroverov, R. Kobayashi, J. Normand, K. Raghavachari, A. Rendell, J. C. Burant, S. S. Iyengar, J. Tomasi, M. Cossi, N. Rega, J. M. Millam, M. Klene, J. E. Knox, J. B. Cross, Bakken, C. Adamo, J. Jaramillo, R. Gomperts, R. E. Stratmann, O. Yazyev, A. J. Austin, R. Cammi, C. Pomelli, J. W. Ochterski, R. L. Martin, K. Morokuma, V. G. Zakrzewski, G. A. Voth, P. Salvador, J. J. Dannenberg, S. Dapprich, A. D. Daniels, Ö. Farkas, J. B. Foresman, J. V. Ortiz,

- J. Cioslowski and D. J. Fox, Gaussian09 Revision E.01, Gaussian Inc., Wallingford CT, 2009.
- 23 C. M. Western, J. Quant. Spectrosc. Radiat. Transfer, 2017, 186, 221-242.
- 24 H. Pickett, J. Mol. Spectrosc., 1991, 148, 371-377.
- 25 H. Pickett, R. Poynter, E. Cohen, M. Delitsky, J. Pearson and H. Müller, J. Quant. Spectrosc. Radiat. Transfer, 1998, 60, 883-890.
- 26 S. Khemissi, A. P. Salvador and H. V.-L. Nguyen, J. Phys. Chem. A, 2021, 125, 8542-8548.
- 27 L. Ferres, J. Cheung, W. Stahl and H. V.-L. Nguyen, J. Phys. Chem. A, 2019, 123, 3497-3503.
- 28 J. Mélan, S. Khemissi and H. V.-L. Nguyen, Spectrochim. Acta, Part A, 2021, 253, 119564.
- 29 H. Hartwig and H. Dreizler, Z. Naturforsch., A: Phys. Sci., 1996, 51, 923-932.
- 30 I. A. Finneran, J. T. Good, D. B. Holland, P. B. Carroll, M. A. Allodi and G. A. Blake, Phys. Rev. Lett., 2015, 114, 16392.